The Spatial and Temporal Distribution of Nighttime Ozone and Sulfur Dioxide in the Venus Mesosphere as Deduced from SPICAV UV Stellar Occultations

Daria Evdokimova, D. Belyaev, Franck Montmessin, Oleg Korablev, Jean-Loup Bertaux, Loïc Verdier, Franck Lefèvre, Emmanuel Marcq

JGR Planets

RESEARCH ARTICLE
10.1029/2020JE006625

Key Points:

- Ozone density is within 10^7 to 10^8 cm^{-3} in the 85–110 km altitude range from 2006 to 2015
- The altitude profile of the sulfur dioxide volume mixing ratio is vertically uniform around 135 ppbv between 85 and 100 km
- Temporal variations of ozone and sulfur dioxide are analyzed

Supporting Information:

- Figure S1

Correspondence to:
D. Evdokimova,
evd.dar@yandex.ru

Citation:
Evdokimova, D., Belyaev, D., Montmessin, F., Korablev, O., Bertaux, J.-L., Verdier, L., et al. (2021). The spatial and temporal distribution of nighttime ozone and sulfur dioxide in the Venus mesosphere as deduced from SPICAV UV stellar occultations. *Journal of Geophysical Research: Planets*, *126*, e2020JE006625. https://doi.org/10.1029/2020JE006625

Received 16 JUL 2020
Accepted 15 FEB 2021

The Spatial and Temporal Distribution of Nighttime Ozone and Sulfur Dioxide in the Venus Mesosphere as Deduced From SPICAV UV Stellar Occultations

D. Evdokimova[1,2], D. Belyaev[1], F. Montmessin[2], O. Korablev[1], J.-L. Bertaux[2], L. Verdier[2], F. Lefèvre[2], and E. Marcq[2]

[1]Space Research Institute of the Russian Academy of Sciences (IKI), Moscow, Russia, [2]LATMOS, CNRS, Sorbonne Université, UVSQ, Guyancourt, France

Abstract The nighttime ozone and sulfur dioxide distributions were analyzed using the entire Spectroscopy for the Investigation of the Characteristics of the Atmosphere of Venus (SPICAV) UV/Venus Express stellar occultation data set. After the discovery of an ozone layer at 100 km in the mesosphere reported by Montmessin, Bertaux, et al. (2011, https://doi.org/10.1016/j.icarus.2011.08.010), 132 other detections were made during the entire 8 years long observing period of the SPICAV UV instrument. In the rare detections, the peak abundances of O_3 accumulating in the mesosphere are observed with densities from 10^7 to 10^8 molecules·cm^{-3} at 85–110 km. The ozone layer is estimated to vary from 1 to 30 ppbv at 85–95 km while at 95–105 km the volume mixing ratio is expected within an interval from 6 to 120 ppbv. Below 93 km, a puzzling decrease of mixing ratio is observed towards midnight at 30°N. Our work also provides an improved sequel to the analysis of the sulfur dioxide survey previously made in the upper mesosphere by Belyaev, Evdokimova, et al. (2017, https://doi.org/10.1016/j.icarus.2017.05.002). On average, the SO_2 content is found to remain constant throughout the vertical profile at a value of around 135 ± 21 ppbv between 85 and 100 km. Rapid and large variations prevent to conclude firmly on any time or space pattern of SO_2.

Plain Language Summary Observations of light attenuation while bright ultraviolet stars were rising or setting behind Venus permitted us to characterize the quantity of carbon dioxide (the main atmospheric component), sulfur oxide, and ozone between 85 and 110 km of altitude at night. They were performed by the Spectroscopy for the Investigation of the Characteristics of the Atmosphere of Venus (SPICAV) UV instrument on board the ESA Venus Express mission in 2006–2014. For the first time, this data set has been entirely analyzed with the benefit of recent calibration's improvements enabled more faithful restitution of gases' abundances. For ozone, discovered on Venus in 2011, thanks to SPICAV, we have been able to detect maximum concentrations and to estimate its nightside characterization. At midlatitudes, a ratio between ozone and carbon dioxide densities, or O_3 mixing ratio, decreases below 93 km at midnight. This puzzling result is tentatively explained by chemical compounds transported by winds from the dayside hemisphere to the nightside and which are known to quickly react with ozone and destroy it. Sulfur dioxide has been found to vary considerably on a short time scale (days) but, on average, the SO_2 mixing ratio is constant within 85–100 km.

1. Introduction

The mesosphere of Venus is the most active photochemical and dynamical region of the planet. It holds the key of the main components of the sulfur cycle that drives the formation of the thick sulfuric acid cloud layers enshrouding Venus globally. Among the important questions remaining to be addressed is the chemical interactions between several gaseous species that participate in establishing the equilibrium of the major atmospheric chemical cycles. Among these species, sulfur and oxygen-derived compounds occupy the central position. The absence of direct measurements of O_2 in a fundamental state has left a major gap in our appraisal of Venus's atmosphere oxidizing capacity. It is nevertheless possible to gauge this capacity indirectly by probing species related to the presence of oxygen. Ozone is among these species and together with chlorinated species it can expose a substantial fraction of the main reactions presiding to the main chemical cycles.

Ozone on Venus was first discovered by Montmessin, Bertaux, et al. (2011) from the 250-nm absorption Hartley band in Spectroscopy for the Investigation of the Characteristics of the Atmosphere of Venus (SPICAV) UV stellar occultation spectra. It was confidently detected in a few nightside sessions at altitudes ~100 km with local densities of 10^7 to 10^8 cm^{-3}. Before this first detection the ozone presence was predicted by photochemical models (Krasnopolsky, 2010; Mills et al., 2006; Yung & DeMore, 1999). More recently, an analysis of SPICAV UV nadir dayside observations have established an abundance of O_3 of 10–20 ppbv at the cloud top (~70 km) in the polar regions (Marcq, Baggio, et al., 2019), in agreement with Venus' atmosphere general circulation simulations (Lebonnois et al., 2010). This detection in nadir geometry provides access to the column-abundance of ozone above the cloud layer. The total ozone amount above the clouds is about 0.1–0.5 Dobson units (1 DU is equivalent to 2.69×10^{16} molecules per cm^2 or to a layer of ozone that would have a thickness of 10 μm under standard terrestrial temperature and pressure) (Marcq, Baggio, et al., 2019) that is ~10 times less abundant than on Mars (Perrier et al., 2006) and $>10^3$ times less than on the Earth.

As for sulfur, it is presumably produced by past or extant volcanic activity and it plays a key role in Venus atmospheric chemistry. An unknown UV absorber at the cloud top diminishing the Venus' albedo has been associated with UV dark sulfur compounds (Frandsen et al., 2016; Krasnopolsky, 2006, 2017, 2018). Sulfur dioxide (SO_2) is the third most abundant gas in the Venus atmosphere. The oxidation of SO_2 and further reaction with water vapor leads to the formation of cloud aerosol particles consisting of a 75%–80% H_2SO_4 water solution (Esposito et al., 1983). Thus, any significant variations of SO_2 abundance occurring in the upper atmosphere are an indicator of a change in the global photochemical processes and/or dynamics on Venus.

The historical record of sulfur dioxide observations on Venus started in 1979 (Barker, 1979) reveals significant variations of its amount in time and space (see details on the SO_2 vertical distribution in a survey of Vandaele et al., 2017a and on SO_2 temporal and spatial variations in Vandaele et al., 2017b). However, the SO_2 was mainly watched in the daytime atmosphere. By now, the first stellar occultation experiment performed by the SPICAV UV spectrometer on board the Venus Express spacecraft provided the most detailed data set to study the SO_2 night content over clouds. It was accompanied by solar occultations executed in IR and UV (SOIR/SPICAV UV) for a detailed study of the vertical distribution of minor species at morning/evening terminators in two ranges of 65–80 and 85–105 km correspondingly. A minimum SO_2 abundance of about 60 ppbv was detected at 70–80 km with an average variability of 80% (Mahieux et al., 2015). Over 85 km, on average, measured SO_2 volume mixing ratio (VMR) increased with altitude from 8–20 ppbv at 85–90 km to 50–180 ppbv at 100 km (Belyaev, Evdokimova, et al., 2017; Belyaev, Montmessin, et al., 2012). The analysis of SO_2 content in the night upper mesosphere revealed 3–4 times higher abundance at the midnight than one observed at the twilight at ~95 km and the smoothing of the difference at altitudes lower 95 km (Belyaev, Evdokimova, et al., 2017). The long-term variations at night and terminators showed some sporadic maxima, however, they did not identify any trend at 90–95 km.

In this work, we are completing the previous analysis of the stellar occultation data obtained by SPICAV UV which was aimed to study the SO_2 variations (Belyaev, Evdokimova, et al., 2017) and the first ozone detection in the night upper mesosphere of Venus (Montmessin, Bertaux, et al., 2011). Compared to these previous works, the present analysis is based on an improved calibration scheme described in Evdokimova et al. (2020). It also takes into consideration the entire stellar occultation data set of SPICAV collected between 2006 and 2014.

2. Description of the Data Set

The ultraviolet channel of the SPICAV spectrometer on board the Venus Express spacecraft (Bertaux, Vandaele, et al., 2007) has been orbiting around Venus from April 2006 to December 2014. A unique corpus of stellar occultation data in the UV was collected in the mesosphere, composed of 690 observations performed on the nightside of both hemispheres. The analysis of SPICAV UV spectra collected in the 118–320 nm wavelength range with a 1.5-nm resolution has provided retrievals of CO_2 density and temperature (Piccialli et al., 2015). This range includes absorption bands of carbon dioxide (118–200 nm), sulfur dioxide (180–220 and 250–290 nm), and sulfur monoxide (190–220 nm), as well as Hartley's absorption band of ozone (220–280 nm).

SPICAV regularly performed observations in the stellar occultation mode for the entire 8-year period of the Venus Express mission. In this work we analyze the complete data set of those measurements accumulated from June 2006 to December 2014. On the dayside the high intensity of the scattered solar radiation prohibits the use of the stellar occultation mode. For this reason all data collected at a tangent point with a solar-zenith angle (SZA) smaller or equal to 95° were excluded from our analysis. Six hundred and ninety occultations were made on the nightside. SPICAV observed 58 different bright UV stars that were permitted to cover all longitudes and latitudes from 80°S to 80°N.

The stellar occultation is effective above the opaque aerosol haze located at 70–85 km (Esposito et al., 1983; Luginin et al., 2016) and below 150 km which corresponds to the upper mesosphere (Belyaev, Evdokimova, et al., 2017; Montmessin, Bertaux, et al., 2011; Piccialli et al., 2015). In addition to the observed gaseous absorption, the spectrometer coregisters UV emissions from the nitrogen oxide airglow at 190–270 nm and the scattered radiation in the Lyman-alpha at 121.6 nm. Thus, the preliminary step of data processing concerns the separation of the atmospheric absorption spectra from the UV emission spectra. One more preprocessing step is the wavelength calibration improved by Evdokimova et al. (2020) and which now compares the reference spectrum of a star measured by SPICAV above 150 km with the same star spectrum found in the IUE catalog (Boggess et al., 1978). Details of the preprocessing procedure are given in Evdokimova et al. (2020). Transmission spectra at altitudes between 85 and 150 km are obtained from ratios of the star spectra measured at these altitudes with the reference spectrum registered above 150 km in the same observation session. Stars, as point sources, permit an accurate determination of the Line of Sight (LOS) geometry. The vertical step between two consecutive transmission spectra varied from 1 to 8 km, and it was defined by the overall geometry of the corresponding occultation. Each transmission spectrum is accompanied by uncertainties which are calculated from raw data error values during the calibration steps (see details on error propagation in Piccialli et al., 2015).

3. Data Analysis

Our analysis yields altitude profiles of SO_2, O_3, and CO_2 at every altitude probed during the occultation sequence. Absorption by SO overlaps the SO_2 band but the spectral resolution of SPICAV prevents its separation from SO_2, the main absorber. We consider a fixed ratio between sulfur monoxide and sulfur dioxide of 1/50 which is based on microwave observations (Sandor et al., 2010) of the nighttime mesosphere. Absorption by CO_2, SO_2, SO, and O_3 is the product of the gas wavelength-dependent cross sections with their local density integrated along the instrument LOS. The resulting attenuation of the signal is given by the Beer–Lambert law that states that a source attenuation is equal to the exponential of minus this absorption.

Cross sections of CO_2, SO_2, SO, and O_3 absorption bands used in the analysis are the same as in Montmessin, Bertaux, et al. (2011), Belyaev, Evdokimova, et al. (2017), Marcq, Baggio, et al. (2019), and Marcq, Lea Jessup, et al. (2020). We also considered the effect of Rayleigh scattering in the CO_2-atmosphere, which is significant below 100 km in the UV range (Ityaksov et al., 2008). The spectral slope of the aerosol opacity was approximated by so-called "α-model," where τ_{ref} is a reference value fitted at $\lambda_{ref} = 235$ nm and Angström coefficient α is related to the radii of the H_2SO_4-haze particles (see e.g., Belyaev, Evdokimova, et al., 2017; Wilquet et al., 2009, for details). The α-assumption in the 150–300 nm range was demonstrated equivalent to the Mie theory for the case of Martian aerosols (Määttänen et al., 2013; Montmessin, Quémerais, et al., 2006).

Our fitting routine is based on the adjustment of five atmospheric parameters: slant densities of three gaseous components, CO_2, SO_2, and O_3, and two aerosol parameters τ_{ref} and α. The best fit of the modeled transmission $T_{mod}(\lambda)$ to the measured one $T_{exp}(\lambda)$ was based on the Levenberg–Marquardt algorithm, which searches for the minimum of the χ^2 function by adjusting all five parameters. For each guess of the fitted atmospheric parameters, we estimated the reduced χ^2 value: $\chi^2 = \Sigma[(T_{exp}(\lambda_i) - T_{mod}(\lambda_i))/\delta_{exp}(\lambda_i)]^2/N_{free}$ over all the spectral points, where $\delta_{exp}(\lambda_i)$ is the uncertainty of $T_{exp}(\lambda_i)$ and N_{free} is the number of free (fitted) parameters. Retrieved slant concentrations are converted into local densities by the regularized onion-peeling method described in details in Quémerais et al. (2006).

The densities of sulfur dioxide and ozone are close to the detection limit. Thus, the spectral inversion problem was divided into three iterations since the contribution of CO_2 and aerosol continuum absorptions is

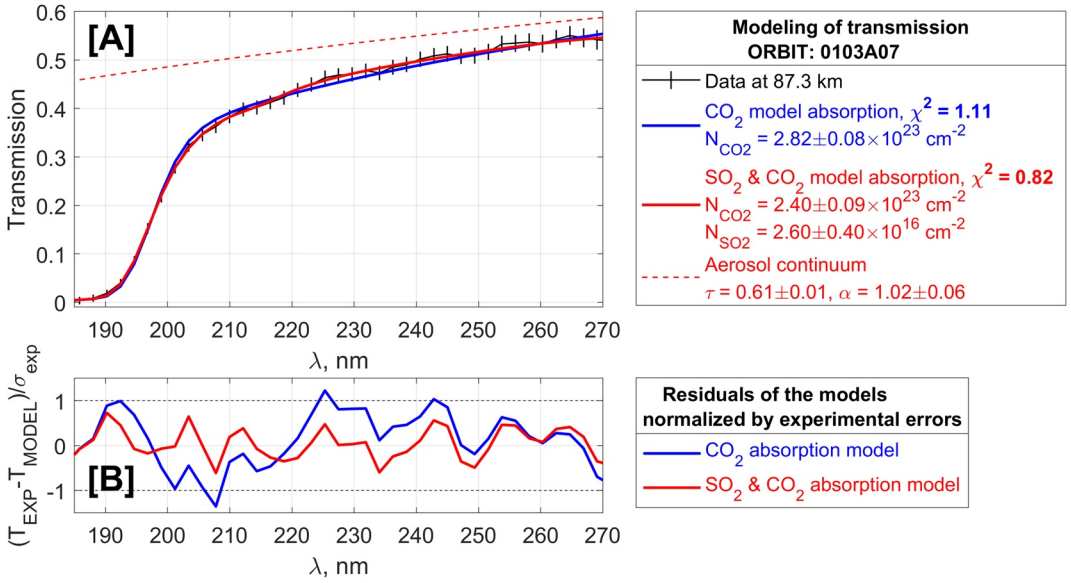

Figure 1. Positive detection of SO_2 at an altitude of 87.3 km in stellar occultation session #0103A07. The observation was done on August 2, 2006, with corresponding parameters: the latitude of −3.9°, the longitude of 241.9° and local time of 23.37 h. (a) Measured transmission spectrum with error bars (black solid curve with error bars); aerosol continuum (red dashed line), modeled transmissions considering absorption of CO_2 (blue solid line), and absorption of CO_2 and SO_2 (red solid line). The synthetic spectra were convolved by the instrumental line shape. (b) Residuals of the difference between the observation and the two different models normalized by the experimental error bars. The blue solid curve corresponds to the model covering the CO_2 absorption. The red solid curve corresponds to the model considering the CO_2 and SO_2 atmospheric absorption. Dashed black lines signify the error bar limits.

much stronger, whereas absorption bands of sulfur and ozone compounds are well separated spectrally. In a first step, three parameters of the CO_2 slant density and the aerosol opacity parameters τ_{ref} and α are retrieved without ozone and sulfur oxides. In a second step, the fourth parameter of the SO_2 slant density is added to the previous iteration set to describe SO_2 and SO absorption. The ozone abundance is still assumed to be equal to 0. In a third step, we add the Hartley band of O_3 absorption to the algorithm. At this point, there are four free parameters relating to SO_2 and O_3 slant densities as well as the aerosol τ_{ref} and α. To reduce the number of free parameters, the CO_2 density is fixed to the value retrieved from the previous best fit. This approach is reasonable since there is no overlap between the O_3 and CO_2 absorption bands in the 150–300 nm wavelength range.

We claim a positive detection of any minor species in the observed spectrum when the χ^2 decreases after adding the SO_2 or O_3 molecular absorptions to the fit. We compare the χ^2 values of best fits at each iteration. The detection is considered positive if the ratio $\chi^2(SO_2, CO_2)/\chi^2(CO_2)$ is lower than 0.95. An example of positive identification of significant sulfur dioxide absorption at an altitude of 87 km is presented in Figure 1a. In this case, χ^2 is reduced by a factor of 0.74. A better correspondence of the model with the SO_2 absorption included is evident when considering residuals normalized to the experimental errors within the SO_2 absorption band of 190–220 nm (Figure 1b).

Ozone absorption describes a spectrum concavity in the range of the Hartley band, that is around 250 nm (Figure 2a), which is placed right between the two SO_2 absorption bands. Therefore, O_3 and SO_2 bands do not interfere with each other and this allows a simultaneous and independent retrieval of SO_2 and O_3 densities (Figure 2a). However, ozone is less abundant than sulfur dioxide in the Venus mesosphere. Moreover, uncertainties in the data increase in this spectral range due to the overlapping emission band of NO (Evdokimova et al., 2020). Thus, the positive detection (Figure 2) criterion was modified with respect to the SO_2 case. In addition to the χ^2 reduction, we analyzed a histogram representing the distribution of the transmission residuals within the Hartley absorption band (Figures 2b and 2c). A proof of the goodness of fit is given when the Gaussian is symmetric about zero. If the histogram fulfills this requirement without considering ozone absorption, we can conclude that ozone is absent from the analyzed spectrum. Conversely,

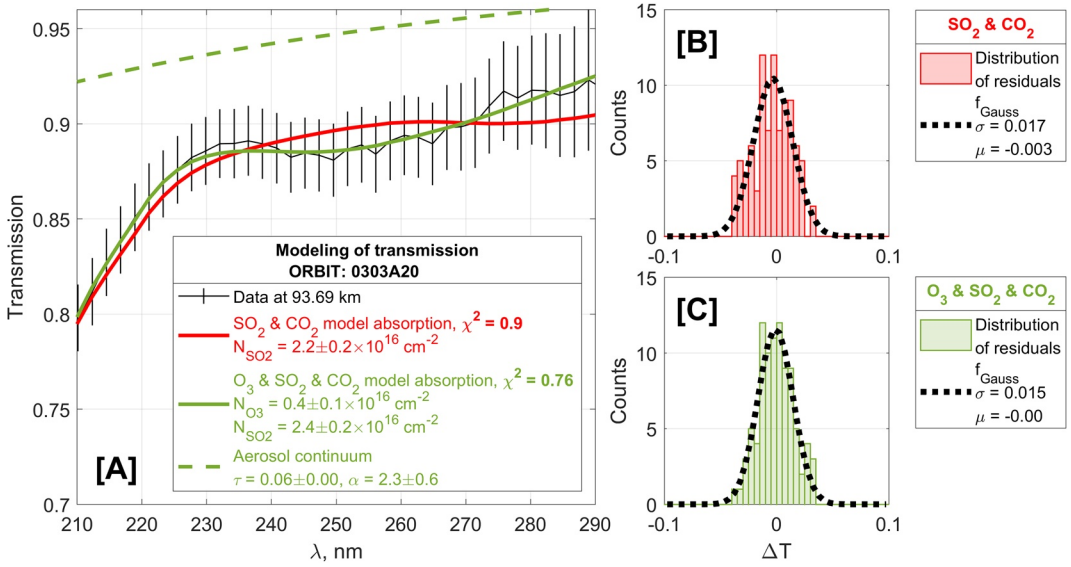

Figure 2. A case of positive O_3 detection at an altitude of 93.69 km in the stellar occultation session #0303A20. The observation was done on February 18, 2007, at the latitude of −11.8°, the longitude of 192.6°, and local time of 20.7 h. (a) Measured transmission spectrum with error bars (black solid line); aerosol absorption (green dashed line); modeled transmissions considering CO_2 and SO_2 absorption (in red) and absorption of CO_2, SO_2, and O_3 (in green). (b and c) Histograms of transmissions residuals. (b) The model without O_3. (c) The model including absorption by three gases.

an offset of the Gaussian maximum would reveal an unaccounted absorption due to ozone, and that the spectrum needs to be fitted with ozone included in the model (Figure 2b). Moreover, the final Gaussian distribution after adding ozone to the retrieval was also checked against symmetry about zero (Figure 2c). To filter out noisy spectra hiding a weak O_3 absorption, we considered only spectra when the mean-width of residual histograms is lower than 0.05.

Both SO_2 and O_3 appear to be highly variable in time, and some observations do not lead to a firm detection. Seventy-five percent of the SO_2 detections correspond to χ^2 reduction of more than 10%. The observed ozone absorption is weaker than SO_2. Only half of the O_3 positive detections corresponds to χ^2 reduction of less than 10%. The mean detection limit of O_3 is estimated to be equal to $(3.3 \pm 0.1) \times 10^{15}$ cm^{-2} within the 90–110 km altitude range. In general, retrieved O_3 concentrations are close to detection limits and do not exceed them by more than a factor of 4. The SO_2 detection limit is $(5.8 \pm 0.2) \times 10^{15}$ cm^{-2} in the 90–110 km range. The SO_2 detection limit is observed at an altitude of about 100 km. Below 100 km, the retrieved SO_2 slant density is 2–10 times higher than the corresponding detection limit. All sessions containing at least one positive detection of SO_2 and O_3 are presented in Figures 3a and 3b correspondingly.

4. Ozone Content Variability

Ozone detection in the night mesosphere of Venus is found to be sporadic. Out of the entire SPICAV-UV data set (690 observations), only 132 sessions delivered at least one positive detection of O_3, that is 154 spectra. Among them, 41% spectra show a confident signature where the χ^2 improvement around the Hartley band is decreased by more than 10% when including ozone. Generally, only one to a few points can be derived from an individual orbit, preventing a detailed study of spatial or temporal variations of ozone content. The positively detected local densities from all observations are grouped in Figure 4. In the observed altitude range, ozone local densities vary between 10^7 and 3×10^8 cm^{-3} depending on altitude. The continuous increase of O_3 VMR equal to a ratio between ozone and carbon dioxide local densities was observed for the whole altitude range. Figure 5 represents statistical distribution of obtained VMR. (All the observational sessions with positive ozone detections are presented individually in Figure S1 in the Supporting information). The median value changes from 10 ppbv at 85 km to 600 ppbv at 108 km. The histograms (Figures 5b.1–5b.6) representing a dispersion of retrieved values within 5-km bins display the low statistics.

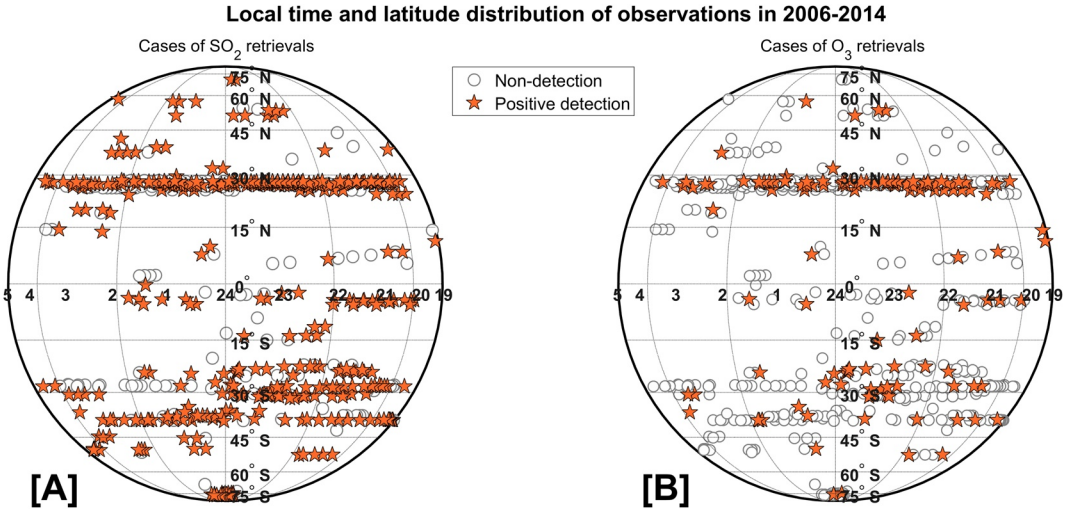

Figure 3. Local time and latitude distribution of observed locations where sulfur dioxide (a) and ozone (b) were detected (pentagrams) and not detected (circles).

The scarcity of ozone detections indicates that the SPICAV UV instrument could only register peak concentrations. A compilation of these values does not represent the mean distribution of O_3 VMR. In fact, the median curve of measured peaks can only represent the profile of the maximum values of O_3 occurring in the nightside mesosphere. The number of ozone occurrences decreases with increasing altitude from 8% at 85–90 km to 4% at 100–105 km. Accounting for nondetections, the mean lower value can be deduced from each 5-km altitude bin. Its value increases with altitude from 1 ppbv at 85–90 km to 6 ppbv at 100–105 km. The area between the minimum and the maximum value profiles is the first estimation to limit the mean vertical profile of O_3 VMR in the night mesosphere (see Figure 9 in Section 6).

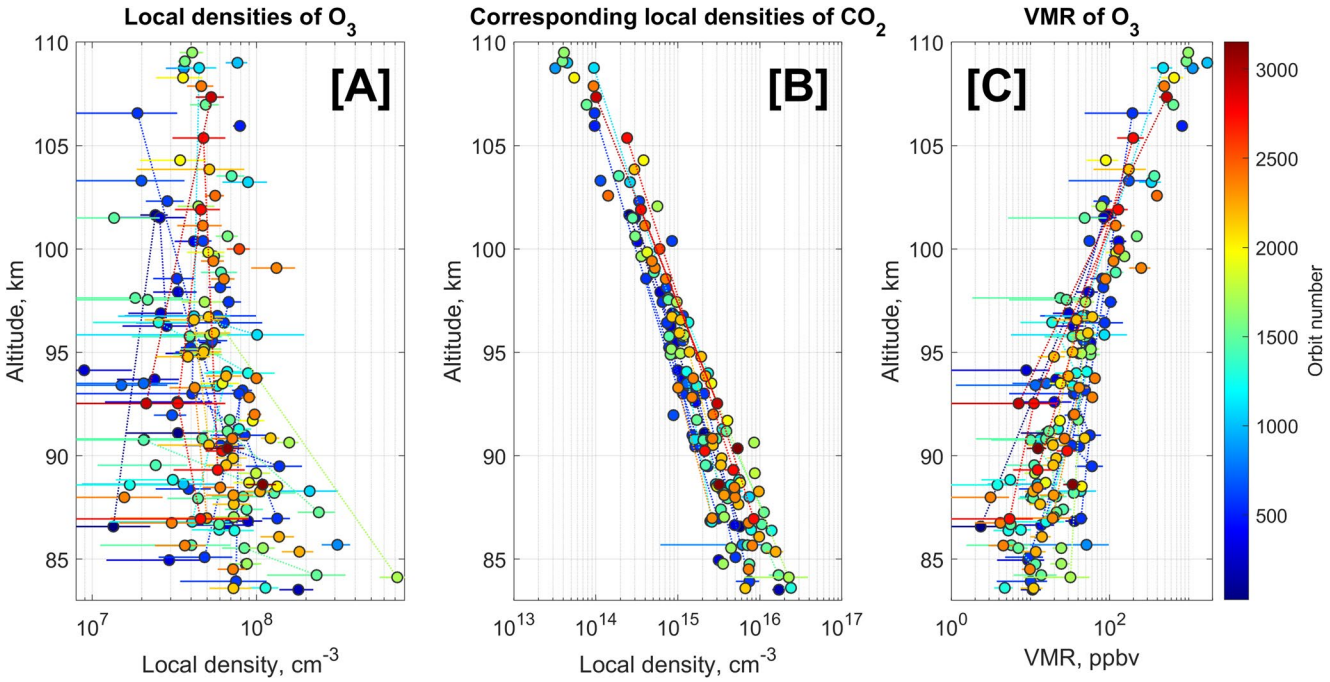

Figure 4. A compilation of ozone positive detections from the entire SPICAV UV data set of 2006–2015. Local densities of O_3 (a), corresponding local densities of CO_2 (b), and ozone volume mixing ratios (c). The color refers to the orbit number of Venus Express. SPICAV, Spectroscopy for the Investigation of the Characteristics of the Atmosphere of Venus.

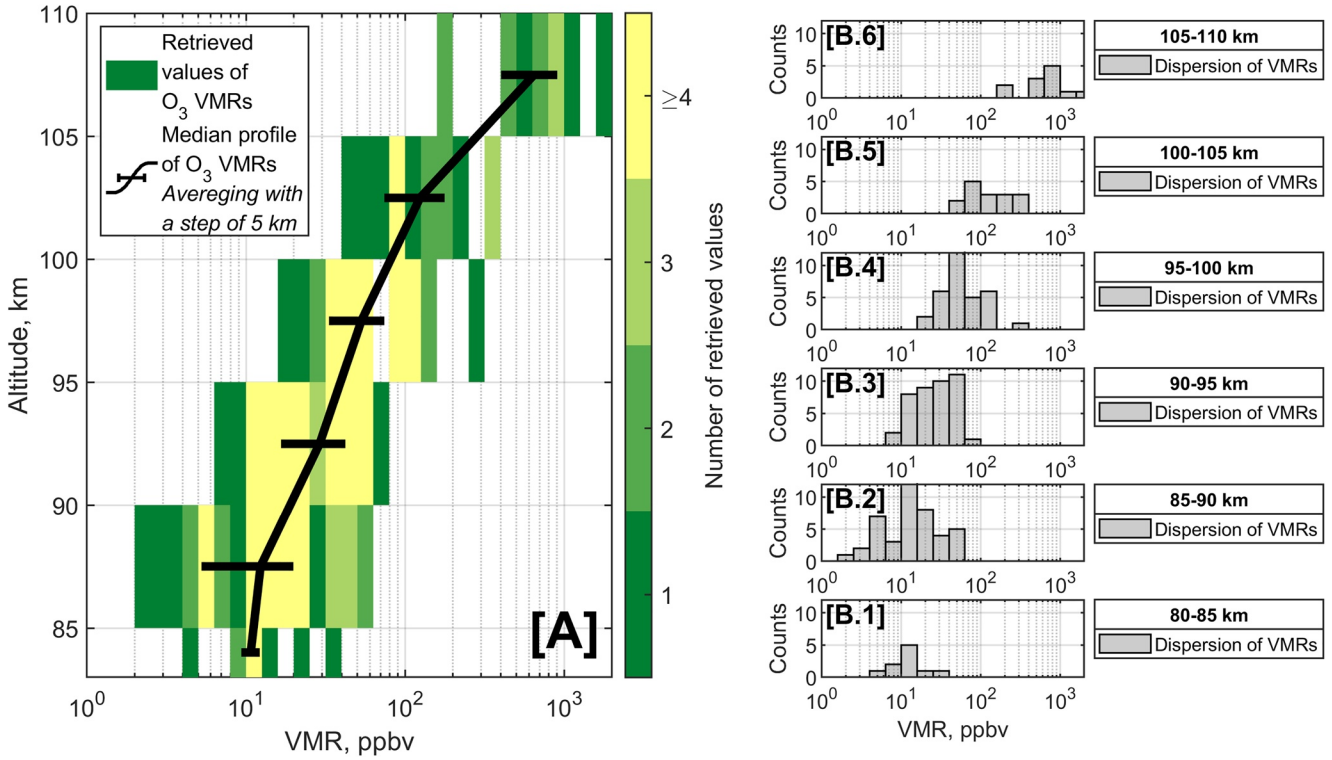

Figure 5. (a) Vertical median profile of the nighttime ozone volume mixing ratio derived from the SPICAV UV observations (the black curve with standard deviation). The color bar indicates the number of points within one bin of 5 km. (b.1–b.6) The right six panels are histograms of values within 5-km bins to represent the stability of the median VMR profile. SPICAV, Spectroscopy for the Investigation of the Characteristics of the Atmosphere of Venus; VMR, volume mixing ratio.

The subsolar to antisolar (SSAS) circulation and subsequent advection of oxygen, hydrogen, and chlorine atoms controls the oxygen chemistry at these altitudes at night (Bertaux, Nevejans, et al., 2007). The reaction between hydrogen and ozone forms OH emission (Bates & Nicolet, 1950; Piccioni et al., 2008). The downwelling oxygen atoms recombine through several processes, producing ozone and excited oxygen molecules that relax to their ground state to form the O_2 ($a^1\Delta_g$) airglow. Both emissions were observed by the VIRTIS instrument of Venus Express. Similarities between O_2 and OH emission profiles were reported (Gérard et al., 2010) with the brightness picked at 96 ± 2 km and the intensities increasing toward the antisolar point. Ozone is expected to follow an opposite trend due to the convergence of reactants in the same area. Nevertheless, Figure 3b demonstrates that the statistics of ozone detections is too poor for an accurate correlation analysis. A few observations made around the antisolar point have not revealed any detection (Figure 3b). Moreover, there is no explicit ozone dependence on latitude and local time.

The densest coverage of detections is found at 20°–40°N latitudes, which allows for a deeper inspection of the local time and long-term variability. Here, the increase of VMRs with altitude is more pronounced around midnight where minimal ozone VMRs below 93 km were obtained. At higher altitudes the minimum disappears (Figure 6a).

The evolution of the ozone mixing ratio at different altitudes through 8 years does not reveal any noticeable trend (Figure 6b). However, some short-term fluctuations of the abundance can be spotted in the time series. This finding indicates that the mesosphere is first and foremost dominated by rapid changes in its composition which may be tied to changes in the circulation, the latter being as the most likely candidate to produce variations of that kind.

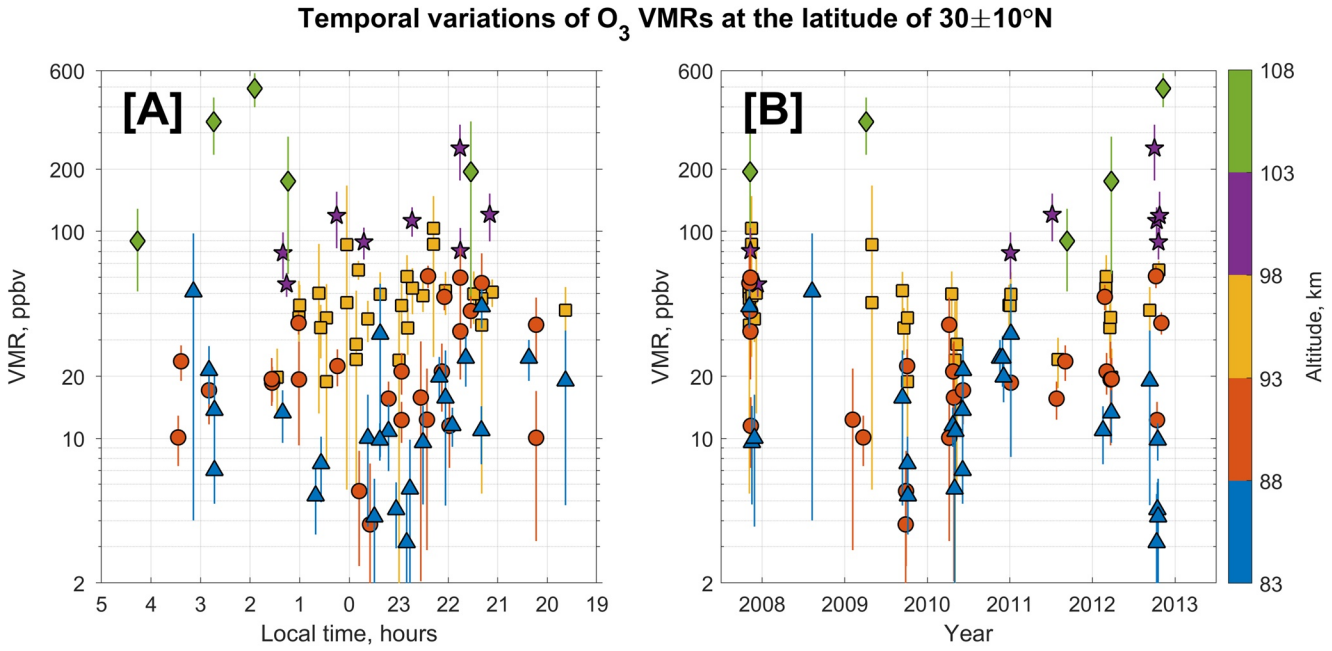

Figure 6. Local time (a) and long-term (b) variability of the ozone volume mixing ratio (ppbv) retrieved at the latitude zone of 30° ± 10°N where the biggest number of observations and detections were obtained. Various colors represent different altitude bins of 5 km.

5. Reanalyzing of the Sulfur Dioxide Distribution

Previously, about 263 observation sessions were reported with CO_2 and SO_2 volume density profiles retrieved within the altitudes of 85–105 km (Belyaev, Evdokimova, et al., 2017). Those stellar occultations correspond to the period from June 2006 to June 2014. In the present paper, we complement these statistics with 110 additional sessions, thus covering the whole Venus Express operating time from June 2006 to December 2014. The analysis of SO_2 variations was performed based on 373 retrieved altitude profiles, in general, constituted by two or more points over 83 km. Our data set has been produced with the improved data processing algorithm described in Evdokimova et al. (2020).

The SO_2 abundance shows significant variability. The VMR retrieved from different observational sessions can differ by up to 1 order of magnitude. This variability is not explained by data uncertainties. On average, the derived SO_2 VMRs feature has a relative uncertainty of about 30%. Figure 7a presents the vertical distribution of the SO_2 VMR which fluctuates around a median value of about 135 ppbv. SO_2 VMRs were grouped in 2 km altitude bins to compute the local median. In the altitude range from 84 to 100 km, the VMR is nearly constant around 120–160 ppb, while above 100 km it increases up to 300 ppbv. However, this altitude interval is marked by a sharp reduction of the number of retrieved values as the detection limit is approached (Figure 7b). The majority of SO_2 detections are found in the altitude range from 85 to 100 km. Above 100 km, the number of retrievals per histogram element is smaller than 10. The behavior of the SO_2 vertical mixing ratio profile differs from the previously reported increase with altitude (Belyaev, Evdokimova, et al., 2017), where values were found to increase from 20 ± 10 ppbv at 85–95 km to 200 ± 100 ppbv at 100–105 km. This correction discussed in Section 6.2 is determined by a sensitivity of the retrieved CO_2 concentration to the accuracy of the wavelength-to-pixel assignment which was improved since and was described in Evdokimova et al. (2020). In addition, the VMR is calculated by dividing the SO_2 density to CO_2 density with both values retrieved simultaneously. Our values of SO_2 VMR display a significant variability. The data set does not cover the nighttime hemisphere in detail (Figure 3a) limiting the scope of our study of the SO_2 spatial distribution. The variations of SO_2 were examined depending on different parameters of the observation: local time, year, and SZA.

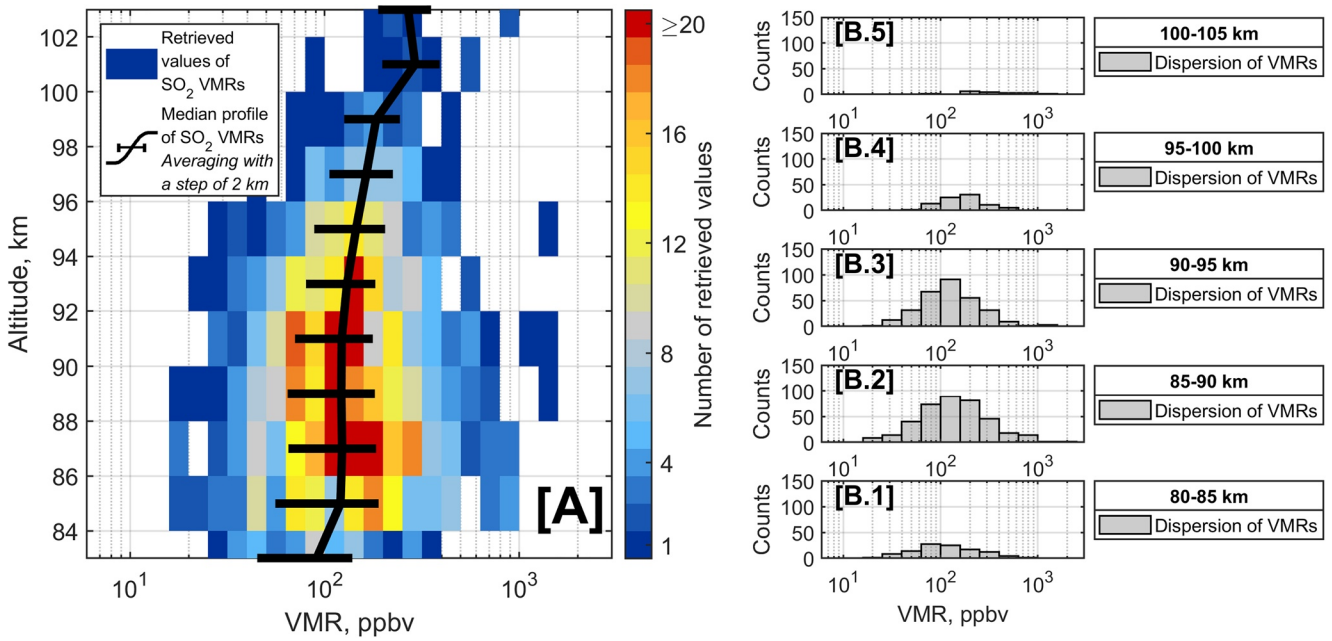

Figure 7. (a) Median profile of nighttime SO_2 volume mixing ratio derived from SPICAV UV (black curve with standard deviation). The colors refer to the number of points included in one bin of 2 km size. (b.1–b.5) The five right panels are histograms representing the distribution of values within bins of 5 km. SPICAV, Spectroscopy for the Investigation of the Characteristics of the Atmosphere of Venus.

5.1. Local Time Variations

The whole data set was analyzed for a local time variability of the SO_2 VMR. The data were splitted by 30 min' intervals. The weighted mean was calculated within each bin. We selected two 5-km thick intervals of 85–90 and 90–95 km where retrieved values are more numerous (see Figures 8b.2 and 8b.3). The analysis considers the number of points constituting the average values in each bin which are represented by histograms below the distribution (Figures 9b.1 and 9b.2). There is a slight VMR decrease suggested from the evening terminator until 02:00 where the VMR changes from 111 ± 36 ppbv at 20:00 to 82 ± 40 ppbv at 02:00 (Figure 9a.2). On the other hand, we do not observe any specific pattern in the 85–90 km range (Figure 9a.1) in frames of the statistical dispersion.

5.2. SZA Variations

We consider only deep nightside observations with SZA > 95°. Unfortunately, the SZA range of 160°–180° is too rarely observed to be statistically significant. Figure 9c presents the VMRs with respect to SZA values, with data divided into 4°-wide bins along the SZA dimension. The weighted-mean values and corresponding standard deviations were calculated within each bin. The minimum of VMRs was noticed in the range of 120°–150° while slightly higher values were measured around 110° for the both altitude intervals (Figures 9c.1 and 9c.2).

5.3. Long-Term Evolution

Long-term variations show strong variability in the sulfur dioxide content (Figure 9e). We analyzed annual variations of SO_2 abundance grouping the values by 1 year' intervals and a weighted mean was computed for each interval. Looking at the variability, one can distinguish two periods of higher VMR values, before 2010 and after that, with a local minimum around 2010. However, for each bin, short-term variations dominate and result in large standard deviations.

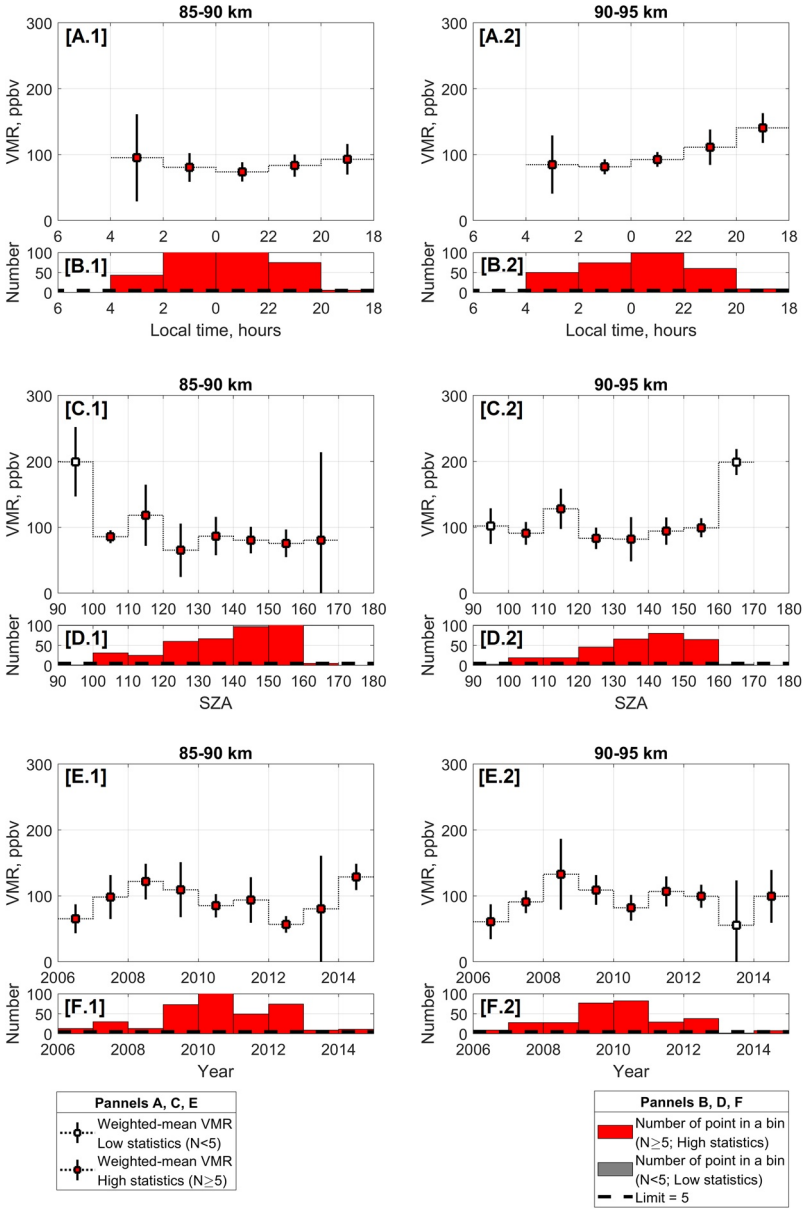

Figure 8. Weighted-mean SO_2 VMR variations with local time (a.1, a.2), solar-zenith angle SZA (c.1, c.2), and year (e.1, e.2) for two altitude ranges of 85–90 km (1) and 90–95 km (2). The data are binned by 2 h of local time, 10° of SZA, and 1 year correspondingly. Red and white square bins with statistical dispersion include ≥5 and <5 individual points respectively. The (b), (d), and (f) panels represent the number of individual points for one bin. Black dashed lines in the histograms correspond to the level of five points. VMR, volume mixing ratio; SZA, solar-zenith angle.

6. Discussion

6.1. Nighttime Ozone Distribution

Ozone was observed during the entire observational period of SPICAV UV. The firm discovery by Montmessin, Bertaux, et al. (2011) at 90–100 km was supplemented by detections at the altitude 85–110 km range. However, in our work, the majority of occultations resulted in a single detection point per ozone profile. Since the observations were done with a vertical step of 1–8 km, a single O_3 occurrence is localized within a narrow altitude interval that should be less than 10 km. Thus, the experiment is only sensitive to peak ozone abundances which are close to the detection limit. The observed values vary by 1 order of magnitude with a slow decrease with height. The slant density of the mean detection limit of 3.3×10^{15} cm^{-2} corresponds to

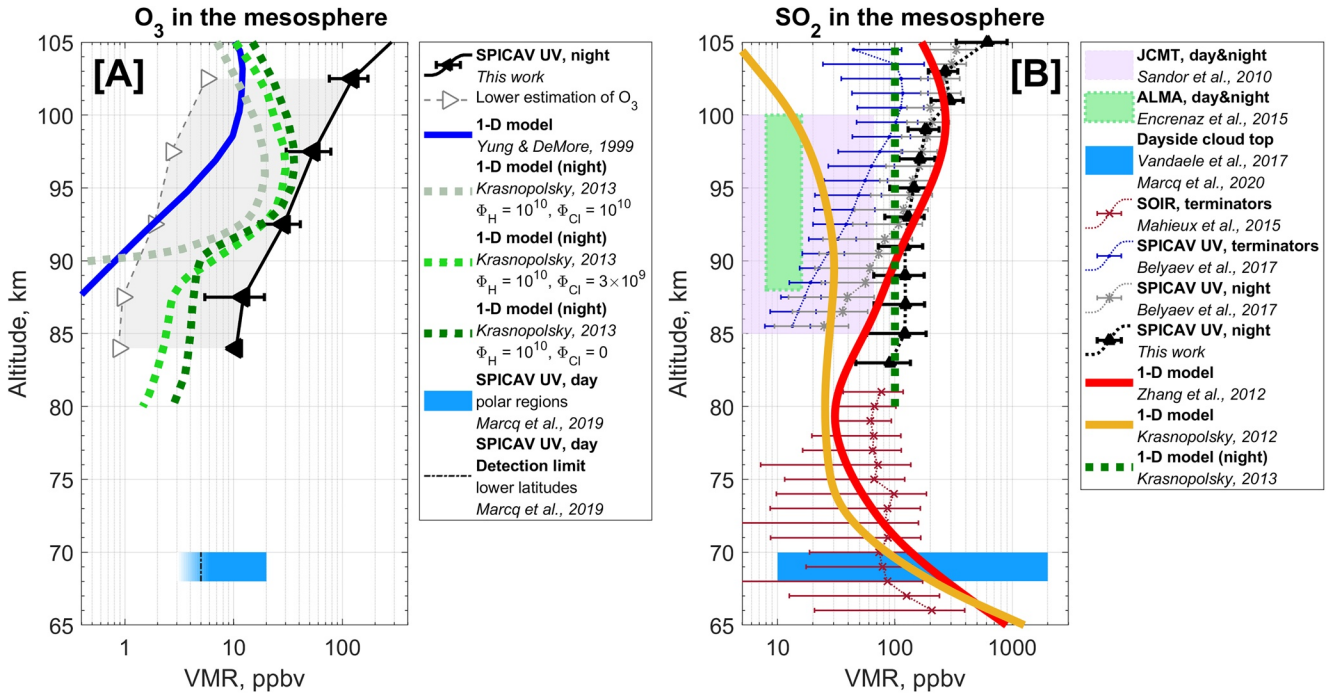

Figure 9. (a) Vertical median profile of the ozone VMR (black triangles) binned by 5 km. Two 1D chemical models are presented: Yung and DeMore (1999) (solid blue line) and Kranopolsky (2013) (dotted lines). The model results of Krasnopolsky (2013) are presented for different chlorine flux conditions. (b) Overview of the sulfur dioxide vertical distributions obtained by different instruments above the clouds. Curve styles and colors are given in the legend box. Three 1D chemical models are presented: Zhang et al. (2012) (red solid line), Krasnopolsky (2012) (yellow solid line), and Krasnopolsky (2013) (green dotted line). The vertical median profile of the SO_2 VMR obtained from this work (black triangles) binned by 2 km. All the occultation results are presented with a dispersion of $\pm 1\sigma$. Cloud top observations of SO_2 and O_3 and the JCMT measurements of SO_2 are represented with the full variety of data. VMR, volume mixing ratio.

~10 ppbv at 90 km and ~100 ppbv at 105 km. In general, this exhibits a pattern of increasing O_3 VMR profile obtained from the SPICAV UV data set (Figure 5a).

Analysis of positive detections' statistics allowed to estimate the lower and upper boundaries for the mean VMR of ozone, which is observed to increase with altitude. Values are enclosed in a range of 1–30 ppbv at 85–90 km and 6–120 ppbv at 100–105 km (Figure 9). The models that predict ozone distribution are consistent with our observations. The 1D photochemical model of Yung and DeMore (1999) describes an increase of ozone from ~1 ppbv at 90 km to a maximum of ~12 ppbv at 100–105 km (Figure 9a) while above 105 km the amount decreases sharply. The nighttime model of Krasnopolsky (2013) considers a chemistry induced by fluxes of O, N, H, and Cl in the upper mesosphere. In particular, it demonstrates an influence of different Cl flux conditions on the ozone production within 80–110 km (Figure 9a). The compiled amount of ozone is about 5–12 × 10^8 cm^{-3} (10–30 ppbv) within the pronounced ozone layer at 90–98 km (Figure 9a). Note that the theoretical behavior of ozone cannot be corroborated by SPICAV UV above 105 km where the number of detections is quite low.

The nighttime behavior of ozone is therefore not reliably established. The few observations performed close to the antisolar point did not provide any detection (Figure 3b). It seems to be the result of a fast ozone destruction process related to the reaction with chlorine radicals transferred to the nightside by the SSAS circulation (Montmessin, Bertaux, et al., 2011). However, the best statistics was accumulated in the midlatitudes of the Northern Hemisphere (30° ± 10°N), which is distant from the antisolar point. Above 93 km, there is no variation with local time. Below, a minimum of VMR is perceptible at 11:00–12:00 p.m., although the weak statistics makes it difficult to firmly conclude on the disappearance of ozone near the antisolar point (Figure 3b). The midnight minimum for O_3 below 88 km (Figure 6a) around the 30°N latitude might be also considered as the effect of mesospheric circulation pattern. The difference in altitude between the

airglow peaks and the ozone minimum is puzzling, yet may reveal the time scale involved for forming and then destroying (both with H and Cl) the bulk of O_3 as the air masses plunge deeper.

6.2. Sulfur Dioxide Distribution

On average, the SO_2 VMR profile is found to remain around 135 ± 21 ppbv in the altitude range of 85–100 km. This value is at least 2 times higher than the maximum VMR = 66 ± 2 ppbv at 85–100 km obtained by the JCMT ground-based observations (Sandor et al., 2010). A smaller value, 12 ± 4 ppbv in 70–100 km was reported by millimeter and submillimeter ALMA observations (Encrenaz et al., 2015), more in agreement with Belyaev, Evdokimova, et al. (2017) values at the terminator (Figure 9) obtained in the solar occultation mode around the Northern pole.

There are no other SO_2 observations in the same altitude range. Sandor et al. (2010) showed that the SO_2 abundance in the 85–100 km range is much larger than in the 80–85 km range, suggesting the presence of a strong sink of SO_2 below 85 km. Below 83–85 km, the atmosphere becomes opaque for the UV stellar occultation to infer SO_2 behavior. Both morning and evening terminators were also investigated by the solar occultation experiment SOIR on board Venus Express in the IR. It was sensitive to observe SO_2 abundance in the 65–80 km range (Mahieux et al., 2015). A minimum of about 60 ppbv was detected at 70–80 km with significant variability (~80%). Unfortunately, probing the 65–85 km region was only possible near the terminator but not on the night side.

A possible local time asymmetry was observed in the range of 90–95 km where VMRs seem to decrease from evening to morning. Such behavior is questionable. It should be noticed that a similar asymmetry was recently deduced from a study of the Venusian atmospheric circulation in the 90–110 km range based on tracking the O_2 ($a^1\Delta_g$) airglow features (Gorinov et al., 2018). As it was shown, velocities of two opposite flows in zonal directions from evening and morning terminators toward midnight reach zero values around 22.5 ± 0.5 h. This asymmetry in the zonal flow would affect chemical species involved in SO_2 photochemistry, such as chlorinated species and oxygen atoms.

Our revised values of the sulfur dioxide VMR do not exhibit a clear increase with altitude as reported previously (Belyaev, Evdokimova, et al., 2017). Significant improvements have been added to the data processing since this earlier work. In particular, the retrieved CO_2 abundances are very sensitive to wavelength calibration which received a major rework (Evdokimova et al., 2020). This has deeply affected SO_2 VMR where CO_2 absorption saturates. This explains why the main differences between the older and the updated SO_2 retrieval are located below 95 km, whereas above SO_2 VMRs are in agreement. However, at 85 km, the difference between our estimates and those of Belyaev, Evdokimova, et al. (2017) reaches a factor of 10. It should be mentioned that calibration improvements could not be implemented to solar occultations presented by Belyaev, Evdokimova, et al. (2017), since the wavelength registration and UV emissions' signal elimination are treated differently between solar and stellar occultations.

7. Conclusions

The current analysis is aimed to examine the O_3 and SO_2 content in the Venus upper mesosphere (85–110 km) at night. Both species were simultaneously retrieved from the entire stellar occultation data set of atmospheric transmission spectra obtained by SPICAV UV on board Venus Express. Data corresponds to SZAs exceeding 95° and covers local times from ~18:00 to ~06:00. We conclude the following results:

(1) For the first time, ozone in the night atmosphere of Venus was monitored for 8 years and was detected in 132 observations. A low amount was retrieved, with local concentrations decreasing from 10^8 to 10^7 cm^{-3} at 85–110 km. The retrieved values correspond to peak ozone concentrations while, in general, each detection constitutes a single point per profile.
(2) O_3 VMR can be estimated in the 85–105 km range considering the detection limits and the number of positive detections. The derived value corresponds to an interval from 1 to 30 ppbv at altitudes of 85–95 km while at 95–105 km the VMR is between 6 and 120 ppbv. The ozone mixing ratio is increasing with altitude.

(3) Ozone detections are sporadic. Individual observations show significant changes in VMR in time and space. Temporal variations were studied in detail in a latitude zone of 30°N±10° where the best coverage was achieved. The local time distribution of ozone content might show a dependence with altitude. Below 93 km, there may be a decrease toward midnight from the terminators. This minimum flattens higher up in the mesosphere. The pattern is presented only for the 30°N-latitude zone where the observation statistics is dominant. The long-term variations, in turn, did not reveal any significant trends.

(4) The median VMR of SO_2 remains around 135 ± 21 ppbv in the range of 85–100 km. In comparison with the previous study of Belyaev, Evdokimova, et al. (2017), a smaller vertical gradient of SO_2 volume density was found. The change of values is strongly related to the improved calibration method that now enables the derivation of more consistent CO_2 concentration values and thus of the relative mixing ratios of trace gases. This reanalysis includes improved calibrations implemented from Evdokimova et al. (2020).

(5) Variations of sulfur dioxide content were investigated based on 373 observational sessions. The short-term variations reach one degree in magnitude. In detail, the local time dependence was studied for the interval from 19:00h to 5:00h. A possible local time asymmetry relative to midnight is highlighted. The SO_2 mixing ratio may be decreasing from the evening terminator to 02:00h at the altitude range of 93–97 km.

Data Availability Statement

The retrieved local densities profiles of O_3, SO_2, and CO_2 are available in Mendeley Data (Evdokimova, D. (2020). Sulfur dioxide and ozone in the Venus mesosphere from SPICAV UV stellar occultations, Mendeley Data, V1, https://doi.org/10.17632/3rp533k62w.1). The archive of SPICAV UV/Venus Express observations is available in the Planetary Science Archive of European Space Agency by a link https://archives.esac.esa.int/psa/#!Table%20View/SPICAV=instrument.

Acknowledgments
D. Evdokimova acknowledges support by the French Government Scholarship Vernadski for PhD students. D. Evdokimova, D. Belyaev, and O. Korablev acknowledge support by the Russian Ministry of Science and Higher Education. F. Montmessin, F. Lefèvre, and E. Marcq thank the Program National de Planétologie (PNP) for financial support. SPICAV operations are funded by CNES and Roscosmos.

References

Barker, E. S. (1979). Detection of SO_2 in the UV spectrum of Venus. *Geophysical Research Letters*, *6*(2), 117–120. https://doi.org/10.1029/GL006i002p00117

Bates, D. R., & Nicolet, M. (1950). The photochemistry of atmospheric water vapor. *Journal of Geophysical Research*, *55*(3), 301–327. https://doi.org/10.1029/JZ055i003p00301

Belyaev, D. A., Evdokimova, D. G., Montmessin, F., Bertaux, J. L., Korablev, O. I., Fedorova, A. A., et al. (2017). Night side distribution of SO_2 content in Venus' upper mesosphere. *Icarus*, *294*, 58–71. https://doi.org/10.1016/j.icarus.2017.05.002

Belyaev, D. A., Montmessin, F., Bertaux, J. L., Mahieux, A., Fedorova, A. A., Korablev, O. I., et al. (2012). Vertical profiling of SO_2 and SO above Venus' clouds by SPICAV/SOIR solar occultations. *Icarus*, *217*(2), 740–751. https://doi.org/10.1016/j.icarus.2011.09.025

Bertaux, J. L., Nevejans, D., Korablev, O., Villard, E., Quémerais, E., Neefs, E., et al. (2007). SPICAV on Venus Express: Three spectrometers to study the global structure and composition of the Venus atmosphere. *Planetary and Space Science*, *55*(12), 1673–1700. https://doi.org/10.1016/j.pss.2007.01.016

Bertaux, J. L., Vandaele, A. C., Korablev, O., Villard, E., Fedorova, A., Fussen, D., et al. (2007). A warm layer in Venus' cryosphere and high-altitude measurements of HF, HCl, H_2O and HDO. *Nature*, *450*(7170), 646–649. https://doi.org/10.1038/nature05974

Boggess, A., Bohlin, R. C., Evans, D. C., Freeman, H. R., Gull, T. R., Heap, S. R., & Wilson, R. (1978). In-flight performance of the IUE. *Nature*, *275*(5679), 377–385. https://doi.org/10.1038/275377a0

Encrenaz, T., Moreno, R., Moullet, A., Lellouch, E., & Fouchet, T. (2015). Submillimeter mapping of mesospheric minor species on Venus with ALMA. *Planetary and Space Science*, *113*(114), 275–291. https://doi.org/10.1016/j.pss.2015.01.011

Esposito, L. W., Knollenberg, R. G., Marov, M. Y., Toon, O. B., & Turco, R. P. (1983). The clouds and hazes of Venus. In D. M. Hunten, L. Colin, T. M. Donahue, & V. I. Moroz (Eds.), *Venus* (pp. 484–564). University of Arizona Press.

Evdokimova, D., Belyaev, D., Montmessin, F., Bertaux, J. L., & Korablev, O. (2020). Improved calibrations of the stellar occultation data accumulated by the SPICAV UV onboard Venus Express. *Planetary and Space Science*, *184*. https://doi.org/10.1016/j.pss.2020.104868

Frandsen, B. N., Wennberg, P. O., & Kjaergaard, H. G. (2016). Identification of OSSO as a near-UV absorber in the Venusian atmosphere. *Geophysical Research Letters*, *43*, 11146–11155. https://doi.org/10.1002/2016GL070916

Gérard, J. C., Soret, L., Saglam, A., Piccioni, G., & Drossart, P. (2010). The distributions of the OH Meinel and $O_2(a^1\Delta\text{“}-\text{”}X^3\Sigma)$ nightglow emissions in the Venus mesosphere based on VIRTIS observations. *Advances in Space Research*, *45*(10), 1268–1275. https://doi.org/10.1016/j.asr.2010.01.022

Gorinov, D. A., Khatuntsev, I. V., Zasova, L. V., Turin, A. V., & Piccioni, G. (2018). Circulation of Venusian atmosphere at 90–110 km based on apparent motions of the O_2 1.27 μm nightglow from VIRTIS-M (Venus Express) data. *Geophysical Research Letters*, *45*, 2554–2562. https://doi.org/10.1002/2017GL076380

Ityaksov, D., Linnartz, H., & Ubachs, W. (2008). Deep-UV absorption and Rayleigh scattering of carbon dioxide. *Chemical Physics Letters*, *462*(1–3), 31–34. https://doi.org/10.1016/j.cplett.2008.07.049

Krasnopolsky, V. A. (2006). Chemical composition of Venus atmosphere and clouds: Some unsolved problems. *Planetary and Space Science*, *54*(13–14), 1352–1359. https://doi.org/10.1016/j.pss.2006.04.019

Krasnopolsky, V. A. (2010). Venus night airglow: Ground-based detection of OH, observations of O_2 emissions, and photochemical model. *Icarus*, *207*(1), 17–27. https://doi.org/10.1016/j.icarus.2009.10.019

Krasnopolsky V. A. (2012). A photochemical model for the Venus atmosphere at 47–112km. *Icarus*, *218*(1), 230–246. http://doi.org/10.1016/j.icarus.2011.11.012

Krasnopolsky, V. A. (2013). Nighttime photochemical model and night airglow on Venus. *Planetary and Space Science*, *85*, 78–88. https://doi.org/10.1016/j.pss.2013.05.022

Krasnopolsky, V. A. (2017). On the iron chloride aerosol in the clouds of Venus. *Icarus*, *286*, 134–137. https://doi.org/10.1016/j.icarus.2016.10.003

Krasnopolsky, V. A. (2018). Disulfur dioxide and its near-UV absorption in the photochemical model of Venus atmosphere. *Icarus*, *299*, 294–299. https://doi.org/10.1016/j.icarus.2017.08.013

Lebonnois, S., Hourdin, F., Eymet, V., Crespin, A., Fournier, R., & Forget, F. (2010). Superrotation of Venus' atmosphere analyzed with a full general circulation model. *Journal of Geophysical Research*, *115*, E06006. https://doi.org/10.1029/2009JE003458

Luginin, M., Fedorova, A., Belyaev, D., Montmessin, F., Wilquet, V., Korablev, O., et al. (2016). Aerosol properties in the upper haze of Venus from SPICAV IR data. *Icarus*, *277*, 154–170. https://doi.org/10.1016/j.icarus.2016.05.008

Määttänen, A., Listowski, C., Montmessin, F., Maltagliati, L., Reberac, A., Joly, L., & Bertaux, J. L. (2013). A complete climatology of the aerosol vertical distribution on Mars from MEx/SPICAM UV solar occultations. *Icarus*, *223*(2), 892–941. https://doi.org/10.1016/j.icarus.2012.12.001

Mahieux, A., Vandaele, A. C., Robert, S., Wilquet, V., Drummond, R., Chamberlain, S., et al. (2015). Venus mesospheric sulfur dioxide measurement retrieved from SOIR on board Venus Express. *Planetary and Space Science*, *113–114*, 193–204. https://doi.org/10.1016/j.pss.2014.12.011

Marcq, E., Baggio, L., Lefèvre, F., Stolzenbach, A., Montmessin, F., Belyaev, D., et al. (2019). Discovery of cloud top ozone on Venus. *Icarus*, *319*, 491–498. https://doi.org/10.1016/j.icarus.2018.10.006

Marcq, E., Lea Jessup, K., Baggio, L., Encrenaz, T., Lee, Y. J., Montmessin, F., et al. (2020). Climatology of SO_2 and UV absorber at Venus' cloud top from SPICAV-UV nadir dataset. *Icarus*, *335*. https://doi.org/10.1016/j.icarus.2019.07.002

Mills, F. P., Sundaram, M., Slanger, T. G., Allen, M., & Yung, Y. L. (2006). Oxygen chemistry in the Venus middle atmosphere. In W.-H. Ip & A. Bhardwaj (Eds.), *Advances in geoscience. Volume 3: Planetary science (PS)* (pp. 109–117). Singapore: World Scientific Publishing. https://doi.org/10.1142/9789812707192_0012

Montmessin, F., Bertaux, J. L., Lefèvre, F., Marcq, E., Belyaev, D., Gérard, J. C., et al. (2011). A layer of ozone detected in the nightside upper atmosphere of Venus. *Icarus*, *216*(1), 82–85. https://doi.org/10.1016/j.icarus.2011.08.010

Montmessin, F., Quémerais, E., Bertaux, J. L., Korablev, O., Rannou, P., & Lebonnois, S. (2006). Stellar occultations at UV wavelengths by the SPICAM instrument: Retrieval and analysis of Martian haze profiles. *Journal of Geophysical Research*, *111*, E09S09. https://doi.org/10.1029/2005JE002662

Perrier, S., Bertaux, J. L., Lefèvre, F., Lebonnois, S., Korablev, O., Fedorova, A., & Montmessin, F. (2006). Global distribution of total ozone on Mars from SPICAM/MEX UV measurements. *Journal of Geophysical Research*, *111*, E09S06. https://doi.org/10.1029/2006JE002681

Piccialli, A., Montmessin, F., Belyaev, D., Mahieux, A., Fedorova, A., Marcq, E., & Korablev, O. (2015). Thermal structure of Venus nightside upper atmosphere measured by stellar occultations with SPICAV/Venus Express. *Planetary and Space Science*, *113–114*, 321–335. https://doi.org/10.1016/j.pss.2014.12.009

Piccioni, G., Drossart, P., Zasova, L., Migliorini, A., Gérard, J. C., Mills, F. P., et al. (2008). First detection of hydroxyl in the atmosphere of Venus. *Astronomy and Astrophysics*, *483*(3). https://doi.org/10.1051/0004-6361:200809761

Quémerais, E., Bertaux, J.-L., Korablev, O., Dimarellis, E., Cot, C., Sandel, B. R., & Fussen, D. (2006). Stellar occultations observed by SPICAM on Mars Express. *Journal of Geophysical Research*, *111*, E09S04. https://doi.org/10.1029/2005JE002604

Sandor, B. J., Todd Clancy, R., Moriarty-Schieven, G., & Mills, F. P. (2010). Sulfur chemistry in the Venus mesosphere from SO_2 and SO microwave spectra. *Icarus*, *208*(1), 49–60. https://doi.org/10.1016/j.icarus.2010.02.013

Vandaele, A. C., Korablev, O., Belyaev, D., Chamberlain, S., Evdokimova, D., Encrenaz, T., et al. (2017a). Sulfur dioxide in the Venus atmosphere: I. Vertical distribution and variability. *Icarus*, *295*, 16–33. https://doi.org/10.1016/j.icarus.2017.05.003

Vandaele, A. C., Korablev, O., Belyaev, D., Chamberlain, S., Evdokimova, D., Encrenaz, T., et al. (2017b). Sulfur dioxide in the Venus atmosphere: II. Spatial and temporal variability. *Icarus*, *295*, 1–15. https://doi.org/10.1016/j.icarus.2017.05.001

Wilquet, V., Fedorova, A., Montmessin, F., Drummond, R., Mahieux, A., Vandaele, A. C., et al. (2009). Preliminary characterization of the upper haze by SPICAV/SOIR solar Occultation in UV to mid-IR onboard Venus Express. *Journal of Geophysical Research*, *114*, E00B42. https://doi.org/10.1029/2008JE003186

Yung, Y. L., & DeMore, W. B. (1999). *Photochemistry of planetary atmospheres* (p. 306). New York: Oxford University Press. Retrieved from https://ui.adsabs.harvard.edu/abs/1999ppa..conf.....Y/abstract

Zhang, X., Liang, M. C., Mills, F. P., Belyaev, D. A., & Yung, Y. L. (2012). Sulfur chemistry in the middle atmosphere of Venus. *Icarus*, *217*(2), 714–739. https://doi.org/10.1016/j.icarus.2011.06.016